Romanian Reports in Physics, Vol. 64, No. 1, P. 281–293, 2012

ASTROPARTICLE PHYSICS

RADIO TECHNIQUE FOR INVESTIGATING HIGH ENERGY COSMIC NEUTRINOS*

A.M. BADESCU[1], A. SAFTOIU[2], O. FRATU[1], I. BRANCUS[2], B. MITRICA[2], O. SIMA[3], S. HALUNGA[1], G. TOMA[2], I. LAZANU[3]

[1]Faculty of Electronics, Telecommunications and Information Technology, POLITEHNICA University of Bucharest, Bd. Iuliu Maniu, no 1–3, Bucharest, E-mail: alinabadescu@radio.pub.ro
[2] "Horia Hulubei" National Institute for Nuclear Physics and Engineering, P.O.Box MG-6, RO-077125 Bucharest [3]University of Bucharest, Bd. M. Kogalniceanu, nr 36–46, Bucharest

Received November 20, 2010

Abstract. We consider an alternative detection strategy based on coherent radio Cherenkov emission from neutrino-induced showers in natural salt. We present the basic structure of the detector and analyze the characteristics of the radio signal on its propagation from the shower to the antenna. We also study how the pulse couples to the receiver. The behavior of the key instrument-radio antenna is characterized and signal-to-noise ratio limiting situations are also presented.

Key words: electromagnetic shower, neutrino detection, salt.

1. INTRODUCTION

As stable neutral particles, UHE cosmic neutrinos can reach ground level detectors directly from their source (undeflected by intervening magnetic fields), providing information about stars and galaxies. Unlike photons or charged particles [1–6], neutrinos interact very weakly, which makes their observation a scientifical and technical challenge.

Neutrinos can be detected by their interaction products in large volumes of dense, transparent media (ice, salt etc.) by Cherenkov emission. The generated electromagnetic shower (carefully described in [7–11]) produces a net excess of electrons compared to positrons (the effect has been first suggested by Askaryan, [12]) which gives rise to a strong, coherent, radio pulse. The radio power emitted scales inversely with the radiation length of the medium squared and goes like the energy of the primary squared.

* Paper presented at the Annual Scientific Session of Faculty of Physics, University of Bucharest, June 18, 2010, Bucharest-Măgurele, Romania.

Antarctic ice has been the focus of studies for this goal for several years now by the Radio Ice Cherenkov Experiment (RICE) [13], the Antarctic Impulsive Transient Antenna (ANITA) [14] and future Askaryan Radio Array (ARA) [15]. A limit at extremely high neutrino energies has been reported via Fast On-orbit Recording of Transient Events (FORTE) satellite observations of the Greenland ice sheet [16]. There is also another class of experiments searching for Cherenkov emission from UHE neutrinos by neutrino interactions with the lunar regolith-Goldstone Lunar Ultra high energy neutrino Experiment (GLUE) [17].

Recent efforts have concentrated on detection in Salt domes-SAlt bed Shower Array (SALSA) [18]. Salt appears to be even more promising than ice because of the advantage of greater accessibility [19] and the higher density of the medium-which decreases the length of the shower [20].

This is the reason why we are investigating here the possibility to build a large-scale neutrino telescope for detection of UHE cosmic neutrinos in a Romanian salt dome.

We start in Section 1 by presenting some aspects regarding the geometry of the detector and introduce a parameterization of the electric field in order to avoid its time-consuming calculation with the GEANT4 program. The following section analyzes briefly propagation in lossy dielectric media.

Determination of the absolute measured field strength of the showers requires that the antenna effective area, spectral response, coupling efficiency, and angular response all be included in converting the measured voltages to field strengths in the detection medium. These topics are treated in Section 3 and problems concerning signal to noise ratio and energy thresholds are discussed in Section 4. Last section summarizes the results and presents further work.

2. GEOMETRY OF THE DETECTOR AND FIELD PARAMETRIZATION

Because of the large volume and high sensitivities involved, equipment will be configured in multiple radio stations (RS) deployed in a 3D grid. Each RS will include two vertical polarization antennas and two horizontal polarization ones. A pair of antennas (horizontal and vertical polarization), can detect the strengths of electrical field and find its possible direction.

The distance between antennas (operating at hundreds of MHz) should be around 2 m in order to avoid mutual coupling. Each receiving antenna is followed by a notch filter to eliminate the noise, a bandpass filter to select the spectral components, and two low noise amplifiers. The output is recorded in a control center.

Each RS should also incorporate a transmitting antenna for calibration that can be also used for increasing the signal to noise ratio (SNR) and for point

positioning. More to that, cables should be added (for powering, communications and mechanical sustain).

The control center must include devices for hardware triggering, digitization and modulation. The signals from the four receiving antennas are multiplexed and transmitted to surface for further processing. Software triggering is used for elimination of false events. In the end, signals from all antennas are correlated for event reconstruction.

Following [13], [18] and [21], the detector configuration consists of boreholed strings with multiple RS. The pulse generated by the shower is a ring-shaped structure that propagates along the surface of a cone defined by the Cherenkov angle for the medium. On its way it meets the RSs that measure its characteristics. All collected data from all antennas is used to fit the energy and direction of the primary particle.

The RS spacing and also the distance between strings is given by the minimum neutrino energy to be detected, structure of the shower (given by the neutrino type) and the height of the dome. For best performances other factors should be included in optimization programs, like: antenna characteristics, medium properties, signal to noise ratio etc. A symmetrical structure in the *xOy* plane would decrease the processing time.

In order to evaluate the capabilities and potential of the planned experiment to look for neutrinos, one needs a good understanding and comprehensive characterization of the dependence of the radio signal on frequency and observation angle in the media.

Many of the observables of the electric field (*E*-field) spectrum emitted by an electromagnetic shower developing in a dense media, scale to a few percent level with several properties of the media, such as density (ρ), radiation length (X_0), Moliere radius (R_M), critical energy (E_C), and index of refraction (n). Due to that, we will consider a parameterization of the coherent radio pulses from showers [10] that allows us to predict their properties without performing time-consuming Monte Carlo GEANT4 simulations. The parameterization has been derived in the far-field (Fraunhofer) zone. The condition for far-field response are met for a maximum frequency around 10GHz [25].

The E-field spectrum at the Cherenkov angle can be parameterized with the expression [10]:

$$R\left|E(f,R,\theta_c)\right| = 3.2\times10^{-16}\,\frac{E_0}{E_c}\,\frac{X_0}{\rho}\,\frac{f}{1MHz}\,\frac{\sin\theta_c}{1+\left(f/f_R\right)^{1.27}}, \tag{1}$$

where for salt, $X_0 = 22.16\,\mathrm{g\cdot cm^{-2}}$, $\rho = 2.05\ \mathrm{g\cdot cm^{-3}}$, $E_c = 38.5\,\mathrm{MeV}$ and the turnover frequency due to the lateral spread of the shower is f_r=1.7083 GHz.

The field is decreasing linearly with the distance between the shower and antenna and increasing with the operating frequency.

At this point we should mention that [23] found a different parameterization for the electric field:

$$R\left|E(f,R,\theta_C)\right| = 0.52\times 2.53\times 10^{-7}\,\frac{E_0}{1\text{TeV}}\,\frac{f}{f_0}\,\frac{1}{1+\left(f/f_1\right)^{1.44}}, \tag{2}$$

where f_0=1.15GHz and f_1=2.86GHz. The difference between the two parameterizations is presented in Figure 1. It can be noticed that it becomes significant around 10GHz-which will not be the case of our study. In the figure we have also presented the *E*-field at an observation angle of 90 deg. (more details about its calculation can be found in [10]). One can notice that the maximum field value at the Cherenkov angle is achieved for an observation frequency around 1GHz. For different observation angles, the maximum occurs at lower frequencies.

Throughout the rest of this paper we will continue with the parameterization in [10].

The width of the angular distribution of the *E*-field around the Cherenkov angle scales as:

$$\Delta\theta = \frac{c}{f}\,\frac{\rho}{14.95X_0}\,\frac{1}{\sqrt{n^2-1}}, \tag{3}$$

where the refraction index was fixed to $n = 2.45$.

It can be seen that width of the pulse rises as the operating frequency decreases, making lower frequencies more appropriate for detection of radio pulses.

The angular distribution of the pulse around the Cherenkov angle can be parameterized by a Gaussian peak modulated by a $\sin\theta$ which accounts for the angular behavior in the fully coherent region:

$$\left|E(f,R,\theta)\right| = \left|E(f,R,\theta_C)\right|\left[\sin\theta/\sin\theta_C\right]\exp\left(-\left((\theta-\theta_C)/\Delta\theta\right)^2\right). \tag{4}$$

This can be noticed in Fig. 2, where we have presented the observation angles that allow a threshold of 10^{-8} mV/MHz for the E-field generated by a 10TeV particle. The higher frequency (1GHz) is much more restrictive in the sense that the field drops very fast with the observation angle if it is not close to the Cherenkov one.

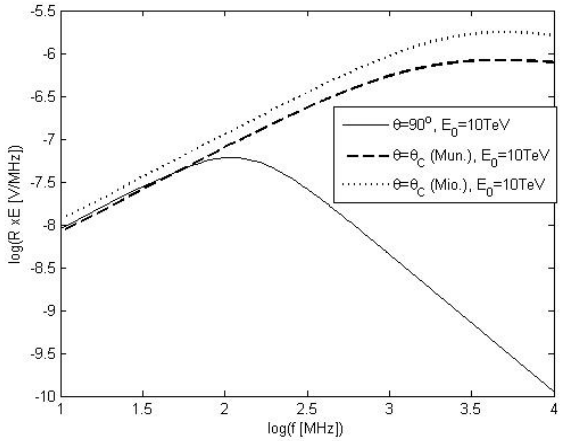

Fig. 1 – The *E*-field generated by a 10TeV particle at the Cherenkov angle as function of the operating frequency. The dashed line describes the parameterization in [10]; the dotted line – the parameterization in [23]. Both cases are at Cherenkov angle. The continuous line presents the parameterization in [10] at an observation angle of 90 deg.

3. PROPAGATION EFFECTS

In the following we will determine how the propagation medium affects the absolute strength of the pulse emitted by the shower.

For propagation in salt domes we can expect no scattering effects and depolarization phenomena [24]. On the other hand, both real $\Re\{\varepsilon_1\}$ and imaginary $\Im\{\varepsilon_1\}$ parts of the permittivity are temperature and frequency dependent [25].

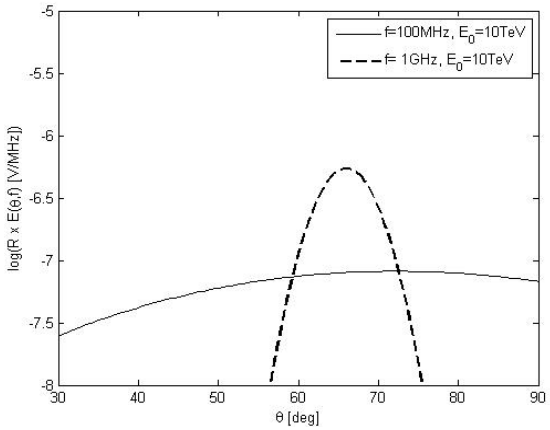

Fig. 2 – The *E*-field generated by a 10TeV particle as function of the observation angle. The dashed line describes a 1 GHz operating frequency; the continuous line – 100 MHz.

As we have no quantitative data yet, we will assume a homogeneous, nondispersive media characterized by a dielectric constant of $\varepsilon_1 = 6 + \mathrm{i}10^{-3}$. The imaginary part of the permittivity is a measure of the absorptions in the medium. The absorption coefficient is given by [24]:

$$\alpha = \left[\pi \sqrt{\Re\{\varepsilon\}} / \lambda_0 \right] \tan\left(\Im\{\varepsilon_1\} / \Re\{\varepsilon_1\} \right). \tag{5}$$

We will determine the effect of impurities in the medium at different frequencies, when the permittivity is $\varepsilon_1 = 6 + \mathrm{i}10^{-5}$ (Fig. 3).

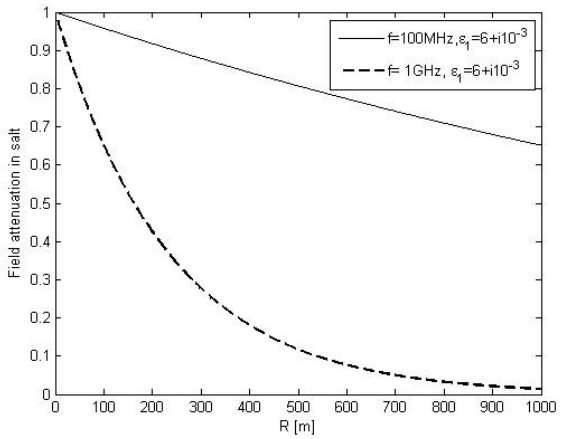

Fig. 3 – The field attenuation as function of the propagation distance. The dashed line represents the situation when f = 100MHz and the continuos one, at 1 GHz.

The second propagation phenomenon to consider are reflexions at separation borders between dielectrics. We will assume that the boreholes that contain the antennas are filled with air.

The electromagnetic radiation travels first in the salt medium and only a fraction of the electric and magnetic fields will cross the interface of separation between the two media (salt/air) while the rest will be reflected backwards and regarded as loss.

The angle that the incident wave makes with the normal at the separation border is a and the angle of the transmitted wave in the second medium is t, connected by Snell's law:

$$\sin a = m \sin t, \tag{6}$$

where m is the ratio of the refractive indexes of salt to air.

For unpolarized incoming radiation, the fraction of the transmitted to incident field from salt to air is given by [26]:

$$T(\varepsilon_1)=\frac{1}{2}\int_0^{\pi/2}\left(\frac{2\cos a}{\cos a+m\cos t}+\frac{2\cos a}{m\cos a+\cos t}\right)\mathrm{d}a, \tag{7}$$

where the first term in the integral represents the vertical polarization and the second, the horizontal one. The modulus is the fraction of the field that is transmitted (if $\varepsilon_1=6+\mathrm{i}10^{-3}$ then $|T|=0.7846$) and the imaginary part - the shift in phase of the electric field. The integral is performed in the $[0,\pi/2]$ interval as the waves enter a medium with a lower refraction index.

4. ANTENNA CHARACTERISTICS

Knowledge of antenna behavior is very important especially as in Ultra Wide Band (UWB) systems conventional methods for characterizing the antenna prove limiting. The need of UWB system is given by the broad band type of the Cherenkov pulse spectrum. In such systems, the antenna acts like a filter so a transfer function must be associated with it [27].

In reception mode, the most promising is the TEM horn that outputs a voltage waveform that is identical to the incident *E*-field. This is because it maintains uniform characteristic impedance [28]. Used with a matched filter and a characteristic impedance of 0.14V/V/m, the detection limit of the energy of the primary particle that generates the shower is a factor of 7 lower than the result obtained with half-wave dipoles in [7].

The major inconvenient is that a TEM horn is highly expensive. The following comes from its shape that makes it hard to handle in underground scenarios.

The antenna transfer function is the ratio of the antenna output voltage V_{rec} to the *E*-field at the antenna $|E_{ant}|$. Its dimension is a length, the so-called effective antenna length [29]. For a dipole antenna, the transfer function is given by:

$$TF_A(f,l,\theta_a)=\sqrt{Z_L/\eta_0}\,|H_{ant}(f,l,\theta_a)|\sqrt{c/4\pi f}, \tag{8}$$

with $\eta_0=377\Omega$ (the intrinsic impedance of free space) and Z_L – the receiver input impedance. *c* is the speed of light in medium (here, air), l is the length of the dipole and θ_a is the angle of incidence with respect to the normal (broadside) of the antenna.

Following [27] one finds that:

$$H_{ant}=F_P(f,l,\theta_a)F_T(f,l), \tag{9}$$

where the pattern term is:

$$F_P(f,l,\theta_a)=\left[\cos\left(\pi f l\cos\theta_a/c\right)-\cos\left(\pi f l/c\right)\right]\Big/\sin\theta_a \tag{10}$$

and

$$F_T(f,l)=\mathrm{j}2\sqrt{\frac{1}{\pi\varepsilon_0 f}}\,\frac{\sqrt{Z_0}}{R_r/\left[\sin\left(\pi f l/c\right)\right]-\mathrm{j}\eta_0\cos\left(\pi f l/c\right)+Z_0\sin\left(\pi f l/c\right)}. \tag{11}$$

Note that $Z_0=50\Omega$ is the characteristic impedance of the port. The term R_r represents the radiation resistance that is dependent on the operating frequency, length of antenna, angle with respect to the normal and current distribution [30]. For a half-way dipole, $R_r=73\Omega$.

The theoretical dependence of the transfer function on θ_a is shown in Fig. 4. One can notice the sidelobes at the higher frequency that will clearly affect the results. Resonance phenomena are expected when considering transfer function variation in frequency.

Considering all presented effects, at the antenna, the pulse will have the form:

$$\begin{aligned}V_{rec}(R,\theta,\varepsilon_1,f,l,\theta_a)=&\sqrt{\varepsilon_1}\,\left|E(f,R,\theta)\right|\times\exp\left[-\alpha(\varepsilon_1)R\right]\times T\left(\varepsilon_1\right)\times\\&\times TF_a(f,l_{ant},\theta_a)\times\cos(\vec{E},TF_a),\end{aligned} \tag{12}$$

where the last term represents the angle between the incoming *E*-field (shifted at the separation border of media) and the angle of incidence with respect to the normal (broadside) of the antenna. As we made no speculations about the direction of the incoming neutrino, we will assume the cosine to be 1.

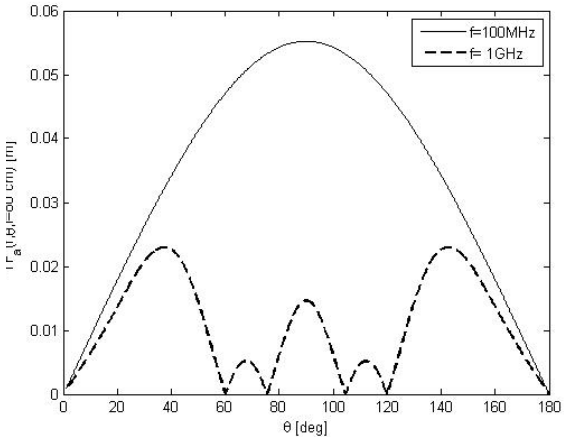

Fig. 4 – Transfer function a dipole antenna of 80 cm with θ_a at two operating frequencies: continuous line-100MHz, dashed line-1GHz.

In Fig. 5 we presented the voltage at the antenna as function of the distance between the shower and the antenna location. We ignored the sidelobes in the transfer function and considered only its maximum value. As expected, it is decreasing with the increase in *R*. On the other hand, one can notice that the observation angle is much more important at higher frequencies (lower panel). The field is also more attenuated at higher frequencies. For a higher energy of the incident particle (10 PeV), the generated *E*-field was four orders of magnitude stronger.

The power delivered to the receiver is maximum if the antenna is folloed by an adapted filter with a matched load impedance, $Z_L(f) = Z_a^*(f)$ where $Z_a{}^*(f)$ represents the complex conjugate of the frequency dependent antenna impedance.

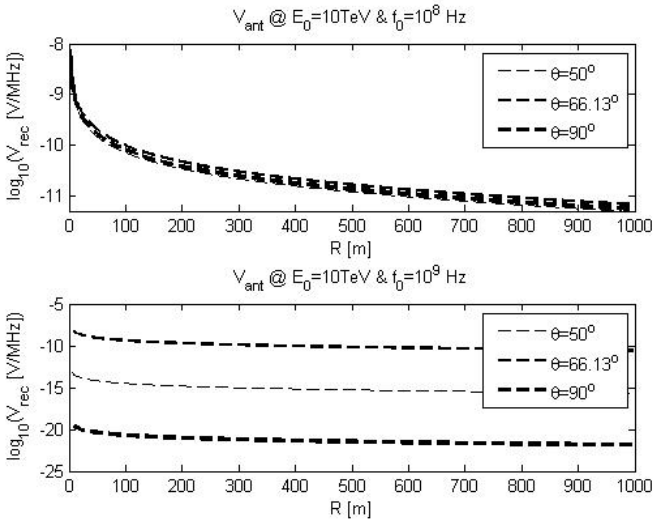

Fig. 5 – Voltage on the antenna as function of the distance between the shower and antenna, for an *E*-field generated by a 10TeV particle. The upper panel presents the situation of an operating frequency of 100MHz and the lower panel, an operating frequency of 1GHz. Both cases present different observation angles: 50 deg. (thin line), 66.13 deg. (thicker line) and 90deg. (thickest line).

Under matched conditions, the voltage delivered to the load is given by:

$$V_m = \left[V_{rec} Z_a^*(f)\right] \Big/ \left[2\Re\{Z_a(f)\}\right] \tag{13}$$

and is presented in Fig. 6. We have chosen to represent it in the frequency interval up to 1.6 GHz as at the turnover frequency f_r=1.7 GHz the waves start to loose their coherency [10].

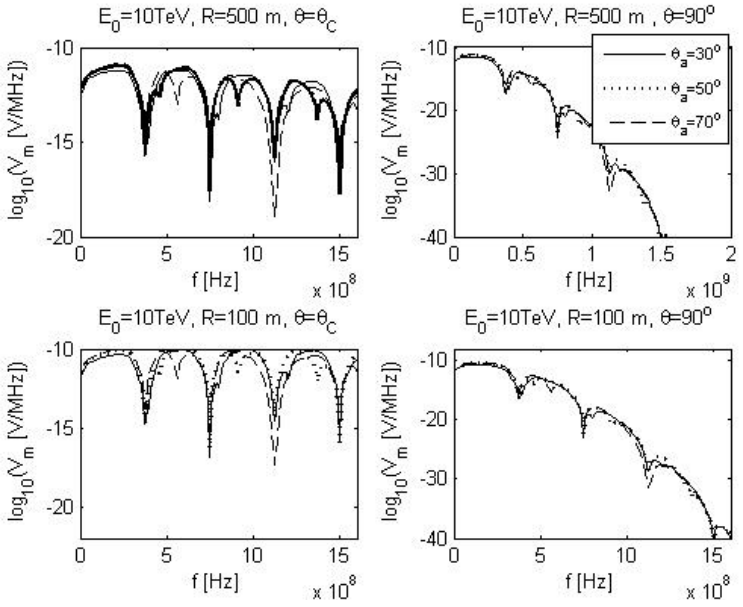

Fig. 6 – Voltage delivered to the load. The upper panels present the situation when the distance between antenna and receiver is 500 m and the lower panel – R = 100 m. The plots on the left side show observations at the Cherenkov angle and the lots on the side show observations at the 90 deg.

5. SIGNAL TO NOISE RATIO

Usually in a system there are more types of noise: Johnson noise generated in the circuitry and the noise given by EM residual fields. In our detector, thermal noise background is neglectable as salt in domes is covered by thick soil, which absorbs electromagnetic wave completely. This way the system is background free from natural or artificial radio waves coming from the surface of the earth and the only contribution to the noise is due to blackbody radiation corresponding to the temperature of the rocks.

Detection of known signal in a white Gaussian noise background is a standard problem of signal processing and is maximized in the sense of maximizing the signal to noise ratio by use of a matched correlation receiver. This way [25]:

$$\mathrm{SNR}^2 = \frac{2}{kT_n}\left(\int_{-\infty}^{\infty} \left|V_m(f)\right|^2 \mathrm{d}f\right)^2 \Bigg/ \int_{-\infty}^{\infty} \left|V_m(f)\right|^2 R_L(f)\mathrm{d}f\,, \tag{14}$$

where R_L is the resistive component of the load impedance Z_L (equal to Z_a^*) and T_n – the system temperature.

We have assumed a system temperature of $T_n = 450\text{K}$ (based on about 310K for the salt and a receiver noise temperature of 140K, consistent with low-noise amplifiers available commercially) and plotted the variation of SNR with the energy of the primary particle (Fig. 7). As expected, SNR is lower at higher distances between source and antenna and also at angles far from Cherenkov angle. For a 10TeV particle, the SNR at θ_C at 1 000m is 46.5 dB, and at 100m–79.09 dB. At θ = 30 deg., SNR=30.74dB. For all angles and distances, the SNR is in the detection limit.

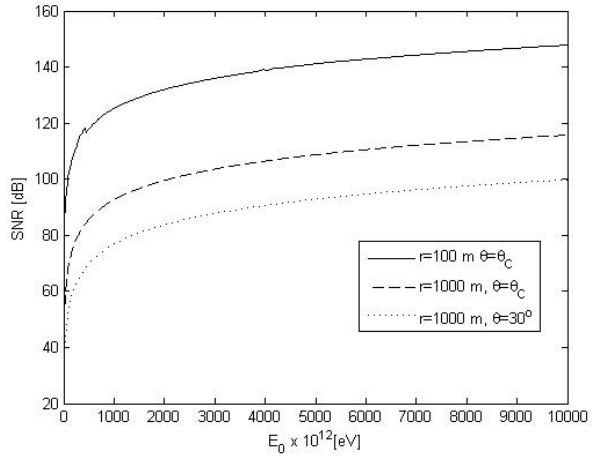

Fig. 7 – SNR as function of the energy of the primary particle. We have presented with a dashed line the SNR at θ_C at 1 000 m; with a continuous line-at 100 m. The dotted line represents SNR at 1 000 m with θ = 30 deg. We have assumed θ_a = 30 deg.

7. CONCLUSIONS

In this paper we have shown that the shower generated field is decreasing linearly with the distance between the shower and antenna and increasing with the operating frequency up to about 1 GHz. On the other hand, the width of the pulse rises as the operating frequency decreases, making lower frequencies (hundred of MHz) more appropriate for detection of radio pulses.

Another argument for observations at lower frequencies is that the antenna transfer function has more side lobes at higher frequencies (for a chosen length of the dipole).

More to that, after considering propagation effects, we proved that at higher frequencies the field gets more attenuated in absolute value and that the variation of the distance between the source and receiving antenna is not producing any considerable effects in the sense that reconstruction of the energy of the primary particle would be impossible.

Last observation is considered to be a disadvantage because the magnitude of the measured field at different distances should have been used in order to reconstruct the direction and energy of the primary particle. Another key point is that at lower frequencies all observation angles are producing similar results. If we would have added the measurement uncertainties, reconstruction of the direction of arrival of the initial particle would become impossible.

The SNR is showing good values at energies above 10TeV, no matter the distance and observation angle.

For an actual design the array parameters such as antenna separation, noise level, operating frequency and bandwidth of each antenna are to be optimized for largest effective volume and minimal cost. The optimization will depend strongly on the shape of the neutrino flux to be measured, but it is clear that higher neutrino sources can allow sparse arrays of antennas in the 100 MHz range and below, which may turn out to be cheaper.

Acknowledgments. A. Badescu is the beneficiary of a grant offered by POSDRU through the POSDRU/6/1.5/S/16 contract. The research activity for this paper was supported by the Romanian Authority of Scientific Research through the 82-104/2008 (DETCOS) project.

REFERENCES

1. A.M. Apostu et al., Rom. Rep. Phys., **63**, 220 (2011).
2. G. Toma et al., Rom. Rep. Phys., **63**, 383 (2011).
3. B. Mitrica, Rom. Rep. Phys., **62**, 750 (2010).
4. M. Cherciu, A.Jipa, Rom. Rep. Phys., **62**, 731 (2010).
5., M. Petrovici et al., Rom J. Phys., **56**, 654 (2011).
6. A. Saftoiu et al., Rom. J. Phys., **56**, 664 (2011).
7. J.Alvarez-Muniz, E. Zas, Phys. Lett. B, **434**, 396 (1998).
8. J.Alvarez-Muniz, R.A.Vazquez, E. Zas, Phys. Rev. D, **62** (2000).
9. J.Alvarez-Muniz, R.A.Vazquez, E. Zas, Phys. Rev D, **61** (2001).
10. J.Alvarez-Muniz, E. Marques, R.A. Vazquez, E. Zas, Phys. Rev. D, **74** (2006).
11. E. Zas, F.Halzen, T.Stanev, Phys. Rev. D, **45**, 362 (1992).
12. G. A. Askaryan, JETP, **14**, 441 (1962).
13. Kravchecko et al., Phys. Rev. D, **73**, 082002 (2006).
14. Silvestri, Proc. Int'l School of Cosmic Ray Astrophysics, astro-ph/0411007, 2004.
15. S. Sun, P. Chen, M.Huang, arXiv:1002.0023v1 (2010).
16. N. Lehtinen et al., Phys. Rev. D, **69**, 013008 (2004).
17. P. W. Gorham et al., Phys. Rev. Lett., **93**, 041101 (2004).
18. A. Connolly, Nucl. Instr. and Meth. A, **604**, 1–2 (2009).
19. M. Chiba, T. Kamijo, O. Yasuda, Y. Chikashige, T. Kon, Y. Takeoka and R. Yoshida, Phys. Atom. Nuclei, **67**, 2050-2053(2004).
20. Lusczeka, E.R., 29th International Cosmic Ray Conference Pune, **8**, *8*, 331334 (2005).
21. B. Hartmann, arXiv:astro-ph/0606697v1 (2006).

22. P. W. Gorham et al., Phys.Rev. D, **72**, 023002 (2005).
23. P. Miocinovic et al., Phys.Rev. D, **74**, 043002 (2006).
24. P.W. Gorham et al., Nucl. Instrum. Meth. A, **490**, (2002).
25. G. Frichter, J. Ralston, D. McKay, Phys.Rev. D, **53**, 1684–1698 (1996).
26. Hapke, *Theory of Reflectance and Emittance Spectroscopy*, Cambridge Univ. Press, 1993.
27. S. Zwierzchowski, P. Jazayeri, Proceedings of Wireless, Calgary, 2003.
28. A.L. Provorov, I.M. Zheleznykh, Astropart.Phys., **4**, 55–62 (1995).
29. O. Kromer et al., Proceedings of the 31st ICRC, ŁODZ 2009.
30. V.F. Fuso, *Foundations of antenna Theory and Techniques*, Pearson Education Limited, London, 2005.